nature physics

ARTICLES

PUBLISHED ONLINE: 30 OCTOBER 2011 | DOI: 10.1038/NPHYS2127

Criticality and isostaticity in fibre networks

Chase P. Broedersz[1,2], Xiaoming Mao[3], Tom C. Lubensky[3]* and Frederick C. MacKintosh[1]*

Disordered fibre networks are the basis of many man-made and natural materials, including structural components of living cells and tissue. The mechanical stability of such networks relies on the bending resistance of the fibres, in contrast to rubbers, which are governed by entropic stretching of polymer segments. Although it is known that fibre networks exhibit collective bending deformations, a fundamental understanding of such deformations and their effects on network mechanics has remained elusive. Here we introduce a lattice-based model of fibrous networks with variable connectivity to elucidate the roles of single-fibre elasticity and network structure. These networks exhibit both a low-connectivity rigidity threshold governed by fibre-bending elasticity and a high-connectivity threshold governed by fibre-stretching elasticity. Whereas the former determines the true onset of network rigidity, we show that the latter exhibits rich zero-temperature critical behaviour, including a crossover between various mechanical regimes along with diverging strain fluctuations and a concomitant diverging correlation length.

Fibrous networks form materials ranging from paper and felt[1,2] to exotic carbon nanotube structures[3,4]. Interconnected networks of filamentous proteins also appear in numerous biological contexts[5–7], including both intracellular mesh-works of actin and microtubules and extracellular matrices of fibrin and collagen[8]. Owing to the collective nature of the softest network deformation modes, the mechanics of such systems depends not only on the elastic properties of the constituent fibres but also sensitively on network connectivity.

It has been known since Maxwell that systems with pairwise, spring-like forces acting between nodes only become rigid above the isostatic connectivity threshold, where the number of constraints arising from such central-force (CF) interactions just balances the number of internal degrees of freedom[9,10]. However, below this CF threshold determined by stretching interactions, networks can be stabilized by extra interactions[11,12], including those arising from fibre bending. Indeed, naturally occurring filamentous networks are known to be rigid at a connectivity below the CF isostatic threshold, suggesting an important role of bending. Nevertheless, the degree to which fibre bending, rather than CF interactions, dominates macroscopic mechanics remains a subject of considerable debate[2,13–22].

Here, we develop both a simulation model and an effective-medium theory, with fibre stretching and bending interactions, to study bond-diluted lattice-based filamentous networks in two and three dimensions (2D and 3D). These networks consist of straight fibres with both stretching and bending rigidity, connected by freely hinged crosslinks enabling free relative rotation of connected fibres. Because the constituent filaments resist stretch and compression, they generate effective central forces directed along the line between crosslinks; and because they resist bending, they generate torques favouring parallel alignment of consecutive segments along a single fibre. We investigate a broad range of network connectivities that covers both the CF isostatic threshold, which marks the onset of network rigidity in the absence of fibre bending stiffness, and a lower-connectivity network rigidity threshold with bending[17,18]. These two thresholds mark rigidity–percolation transitions, placing our model in a broad class of rigidity–percolation models, either with central forces only[11,23] or with extra bending forces[24,25], including those used to model network glasses[10,26,27]. In contrast to those models, here the bending forces act only along a single fibre rather than between fibres.

Our model exhibits non-mean field critical behaviour near the CF isostatic point, like rigidity percolation models but unlike[12] packed spheres near the jamming transition[28–30]. Of particular interest is our finding of a bending-induced crossover at the CF isostatic point, not studied in other rigidity–percolation models and absent from previously studied fibre-network models[17–20,22]. This bending-induced crossover marks the transition between three distinct mechanical regimes: bending dominated, stretching dominated and bend–stretch coupled. The latter regime is characterized by an anomalous power-law dependence of network elasticity both on filament bending and stretching rigidities. These results demonstrate that the fibre's bending rigidity acts as a field that takes the network away from the CF critical point. As further evidence for this critical point, we also find divergent strain fluctuations and a diverging correlation length at the CF isostatic point; on length scales smaller than this correlation length, a continuum elastic description of the network breaks down.

Lattice-based model for fibre networks

We use a combination of simulations and an effective-medium theory to study the elasticity of disordered fibre networks composed of straight and stiff filaments. The network is organized on a bond-diluted triangular lattice in 2D and a face-centred-cubic (fcc) lattice in 3D, as illustrated in Fig. 1a–c. Undiluted, these networks have coordination number $z = 6$ (triangular lattice) and $z = 12$ (fcc), placing them well above the CF isostatic threshold connectivity, $z_{CF} = 2d$, in d dimensions[9,10,12]. In contrast to our model, most previous models for network glasses[10,27,31,32] and stiff-fibre networks[17–20,33] have maximum coordination number 4. We explore the effects of network connectivity—both above and below z_{CF}—by removing filament segments between vertices with a probability $1 - p$.

[1]Department of Physics and Astronomy, Vrije Universiteit, Amsterdam 1081 HV, The Netherlands, [2]Lewis-Sigler Institute for Integrative Genomics and the Department of Physics, Princeton University, Princeton, New Jersey 08544, USA, [3]Department of Physics and Astronomy, University of Pennsylvania, Philadelphia, Pennsylvania 19104, USA. *e-mail: tom@physics.upenn.edu; fcm@nat.vu.nl.

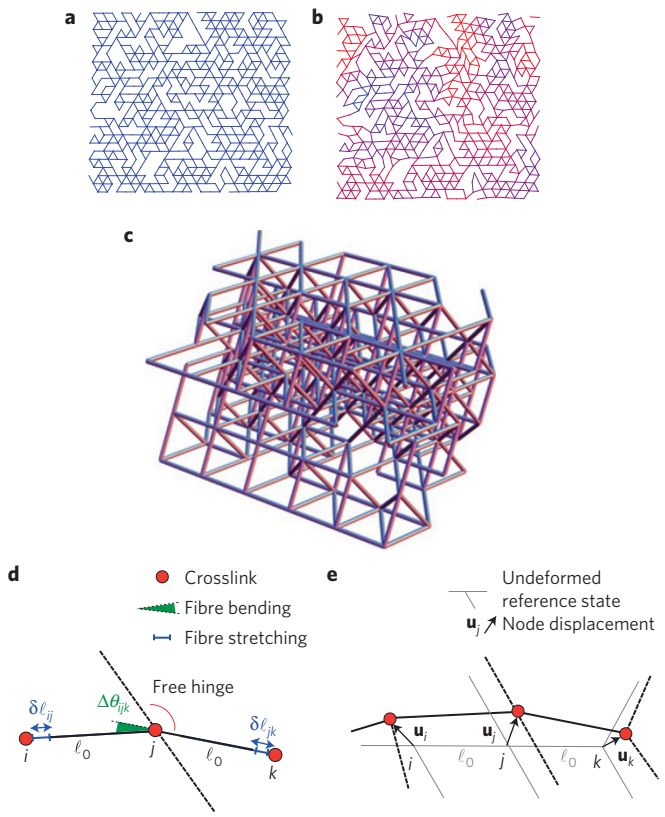

Figure 1 | Fibre networks arranged on lattices in 2D and 3D. a,**b**, A small section of a sheared diluted triangular network near isostaticity with relatively stiff filaments ($\kappa = 10^1$ in units of $\mu\ell_0^2$; **a**) and floppy filaments ($\kappa = 10^{-5}$; **b**). The deviation of the local deformation from a uniform deformation is indicated by colour, where blue corresponds to a uniform or affine deformation and red corresponds to a highly non-affine deformation. **c**, An example of a small section of the diluted fcc network at $p = 0.7$. To probe the mechanical properties of this network we shear the 111 plane (shown on top) along the direction of one of the bonds in this plane. **d**, Schematic representation of two crosslinked fibre segments indicating bond stretching ($\delta\ell_{ij}$) between network nodes and angular deflection ($\Delta\theta_{ijk}$) along consecutive segments on the same fibre. The crosslinks themselves are freely hinged. **e**, Schematic representation of a deformed section of the network. The arrows indicate the deformation of nodes $\mathbf{u}_i$ with respect to the undeformed reference state.

The mechanical energy of the network can be expressed in terms of the stretching and bending contributions of the constituent fibres. The mechanical response of such a fibre is determined by its stretching (that is, Young's) modulus, μ (units of energy/length), and bending rigidity, κ (energy × length). For small deformations, the extension of a fibre segment between vertices i and j is $\delta\ell_{ij} = (\mathbf{u}_j - \mathbf{u}_i)\cdot\hat{\mathbf{r}}_{ij}$ to leading order in $\mathbf{u}_i$, the displacement field of the vertices (Fig. 1d,e). Here, $\hat{\mathbf{r}}_{ij}$ is the unit vector oriented along the i–j bond in the undeformed reference state. Adding all energy contributions resulting from such bond stretching for neighbouring vertices up to quadratic order in the displacements $\mathbf{u}_i$, we arrive at

$$E_{\text{stretch}} = \frac{1}{2}\frac{\mu}{\ell_0}\sum_{\langle ij\rangle} g_{ij}\left(\mathbf{u}_{ij}\cdot\hat{\mathbf{r}}_{ij}\right)^2$$

where ℓ_0 is the lattice spacing, $\mathbf{u}_{ij} = \mathbf{u}_j - \mathbf{u}_i$ and $g_{ij} = 1$ for present bonds and $g_{ij} = 0$ for removed bonds. Importantly, the fibres in this model consist of straight chains of segments with a rest-length ℓ_0. Thus, to calculate the bending contributions to the network's energy, we only consider the change in angle, $\Delta\theta_{ijk} = \theta_{jk} - \theta_{ij}$, for consecutive segments ij and jk along the same fibre in the lattice (Fig. 1d). To leading order, the angular deflection $\Delta\theta_{ijk} = (\mathbf{u}_{jk} - \mathbf{u}_{ij}) \times \hat{\mathbf{r}}_{ij}$, which enables us to express the network's bending energy as

$$E_{\text{bend}} = \frac{1}{2}\frac{\kappa}{\ell_0^3}\sum_{\langle ijk\rangle} g_{ij}g_{jk}\left[\left(\mathbf{u}_{jk} - \mathbf{u}_{ij}\right)\times\hat{\mathbf{r}}_{ij}\right]^2$$

Here, the summation extends only over coaxial neighbouring bonds. Unlike bond-bending[34] and network-glass models[10,27,31,32], the crosslinks at each vertex are freely hinged. Thus, we do not consider crosslinks here that either contribute an extra longitudinal compliance, fix a preferred bond angle or lead to bundling[5,7,16].

Continuous rigidity transitions

To investigate the mechanical response of these fibre networks, we calculate the shear modulus G numerically for networks of size W (see Methods), as shown in Fig. 2a,b. For $\kappa = 0$ (dashed line) the network develops a non-zero macroscopic shear modulus G that grows continuously from zero as $(p - p_{\text{CF}})^{f_{\text{CF}}}$ above the CF threshold, p_{CF}, where $p_{\text{CF}} = 0.651$, $f_{\text{CF}} = 1.4 \pm 0.1$ in 2D, and $p_{\text{CF}} = 0.473$, $f_{\text{CF}} = 1.6 \pm 0.2$ in 3D; the value for the rigidity exponent, f_{CF}, in 2D is consistent with previous work[35]. However, when κ is increased from zero, the rigidity threshold decreases discontinuously to a lower value, p_{b}, which seems to be independent of κ for $\kappa > 0$; again, G grows as a power law, $G \sim (p - p_{\text{b}})^{f_{\text{b}}}$ in the vicinity of p_{b}, where $p_{\text{b}} = 0.445$, $f_{\text{b}} = 3.2 \pm 0.4$ in 2D and $p_{\text{b}} = 0.268$, $f_{\text{b}} = 2.3 \pm 0.2$ in 3D. These values for the bending-rigidity threshold, p_{b}, are consistent with a floppy-mode-counting argument that includes the constraints originating from fibre bending interactions (Supplementary Information). The power-law behaviour of the shear modulus indicates a second-order rigidity transition at both p_{CF} and p_{b}.

The CF threshold marks a crossover between distinct elastic regimes. For $p > p_{\text{CF}}$, G approaches a nearly κ-independent stretching-dominated limit with $G \sim \mu$. In contrast, for $p < p_{\text{CF}}$, G falls off, reaching a bending-dominated limit with $G \sim \kappa$. Interestingly, near p_{CF}, we find a crossover between stretching- and bending-dominated regimes that is characterized by an inflection in G and a strong dependence on the bond occupation probability p, or equivalently, network connectivity. This suggests that the CF isostatic point controls a crossover between the various elastic regimes of fibre networks.

Effective-medium theory and critical crossover

To gain further insight into our model, we characterize the mechanical behaviour of the fibre network, including the crossover near the CF isostatic point, using an analytic approach. In particular, we develop a variation of the effective-medium theory (EMT) for fibre networks with both stretching and bending interactions[36]. This EMT is a mean-field theory that accounts for the disorder in the network by mapping the system to an effective uniform network. The parameters of this effective medium, such as the bending and stretching rigidity of the fibres, are determined by a self-consistency condition on the displacement field on disorder average (see Methods). Conceptually, this amounts to the requirement that the replacement of a single bond in the effective network results in a local distortion of the deformation field, which should average to zero over the full distribution of possible bond replacements. An EMT approach of this form is widely used in the study of disordered systems[37–39], and works remarkably well for the elasticity of disordered lattice models[11,40,41]. Here we go beyond those EMT models by including non-central fibre bending interactions (see Methods).

Our EMT calculation of the shear modulus G in 2D captures the essential features of the network's mechanical response obtained

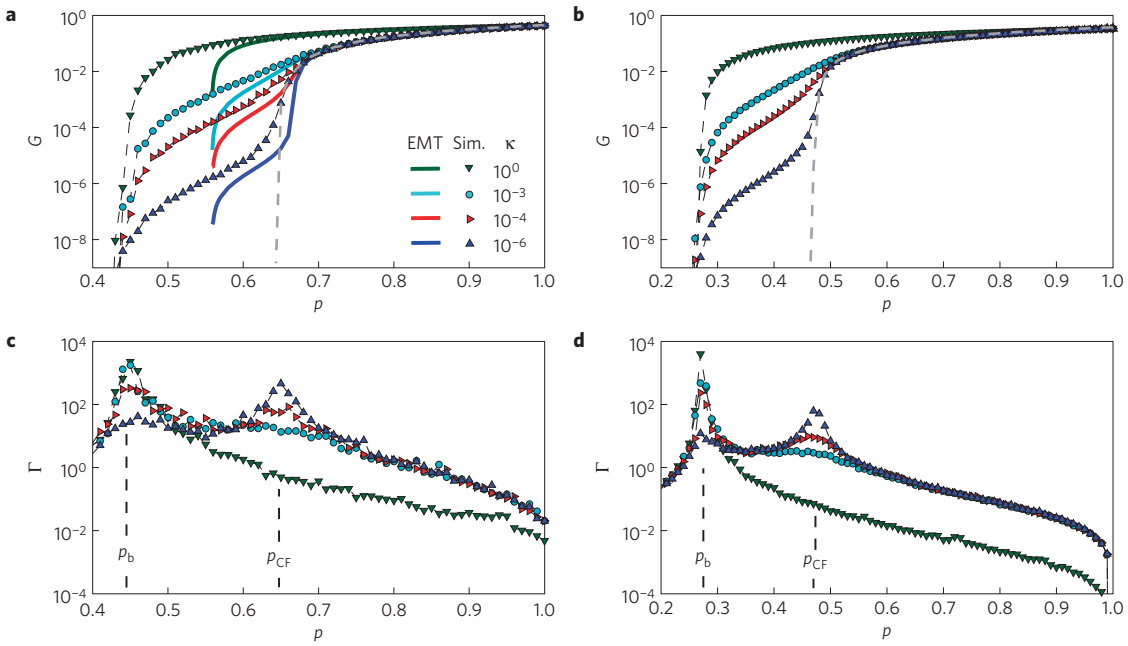

Figure 2 | Mechanics and non-affine strain fluctuations. a,**b**, The shear modulus, G, in units of μ/ℓ_0^{d-1} as a function of the bond occupation probability, p, for a range of filament bending rigidities, κ, for a two-dimensional triangular lattice (**a**) and a three-dimensional fcc lattice (**b**). The numerial results for $\kappa = 0$ are shown as dashed grey lines. The EMT calculations for a two-dimensional triangular lattice are shown as solid lines in **a**. **c**,**d**, The non-affinity measure, Γ, is shown as a function of p for various values of κ for a two-dimensional triangular lattice (**c**) and a three-dimensional fcc lattice (**d**). The values of κ in units of $\mu\ell_0^2$ are 10^0 (green), 10^{-3} (cyan), 10^{-4} (red) and 10^{-6} (blue).

in our numerical simulations, including the existence of separate CF and bending thresholds, as shown in Fig. 2a. The EMT predicts $p_{CF} = 2/3$ and $p_b \approx 0.56$, including a power-law growth of G above the bending threshold with mean-field rigidity exponents $f_b = 1$, and a continuous crossover between stretching- and bending-dominated behaviour in the vicinity of p_{CF}. In particular, for small

$$\Delta p = p - p_{CF}$$

the EMT provides an analytic crossover form for G that highlights the crucial role the CF critical point plays in the bending-induced crossover:

$$G = \frac{\mu}{\ell_0^{d-1}} |\Delta p|^{f_{CF}} \mathcal{G}_{\pm}\left(\frac{\kappa}{\mu\ell_0^2}|\Delta p|^{-\phi}\right) \qquad (1)$$

with mean-field exponents[12] $f_{CF} = 1$ and $\phi = 2$, as shown in Fig. 3a. This scaling form is analogous to that found in random resistor[42–44] and CF spring networks[11] with two types of resistor (or spring) present with respective probabilities p and $1-p$. The universal scaling function $\mathcal{G}_{\pm}(y)$ consists of two branches that together characterize the three regimes of the elastic response of the network. In particular, when $y \ll 1$, $\mathcal{G}_+(y) \sim$ const. and $\mathcal{G}_-(y) \sim y$, implying a stretching regime, $G \sim (\mu/\ell_0^{d-1})|\Delta p|^f$, above the transition, and a bending regime, $G \sim (\kappa/\ell_0^{d+1})|\Delta p|^{f-\phi}$, below the transition. By contrast, in the limit $y \gg 1$, G must become independent of Δp because G is neither zero nor infinite at the transition ($\Delta p = 0$), implying a bend–stretch coupled regime, $G \sim \ell_0^{1-d-2f/\phi}\kappa^{f/\phi}\mu^{1-f/\phi}$, with $f_{CF}/\phi = 1/2$ in the EMT theory.

Our simulations, in both 2D and 3D, indicate a second-order transition (Fig. 3b), characterized by the scaling behaviour in equation (1), but with critical exponents f_{CF} and ϕ ($\phi = 3.0 \pm 0.2$ in 2D and $\phi = 3.6 \pm 0.3$ in 3D) that differ from mean-field predictions (see Table 1). In contrast, spring networks in isostatic configurations near jamming seem to exhibit mean-field behaviour[12]. Furthermore, in the vicinity of p_{CF}, we find a broad crossover regime with an anomalous scaling $G \sim \kappa^x \mu^{1-x}$ (Fig. 3c), where $x = f_{CF}/\phi = 0.50 \pm 0.01$ (2D) and $x = 0.40 \pm 0.01$ (3D). This is in contrast to previous Mikado fibre network models in 2D with $z < 4$, where only pure bending and stretching regimes were identified[17,18]. Interestingly, an anomalous bend–stretch regime similar to what we find here may actually appear when the stretch moduli of the polydisperse segments in such 2D networks are assumed to depend strongly on bond length[45]. Our results for the scaling behaviour of the shear modulus (see equation (1)), including the anomalous scaling of G with κ demonstrated in Fig. 3c, show that κ acts as a field in the critical-phenomenon sense, which takes the system away from criticality and restores network rigidity.

Strain fluctuations and correlation length

To investigate the nature of the various mechanical regimes, we examine the local deformation field in our simulations. Several methods have been proposed to quantify the deviation from a uniform (affine) strain field[17,46,47]. Here we use a measure for this non-affinity given by

$$\Gamma = \frac{1}{N\ell_0^2\gamma^2}\sum_i \left[\mathbf{u}_i - \mathbf{u}_i^{(\mathrm{aff})}\right]^2$$

where $\mathbf{u}_i^{(\mathrm{aff})}$ is the affine displacement of vertex i and N is the number of vertices. This quantity varies over eight orders of magnitude, indicating non-affine fluctuations that depend strongly on both κ and p, as shown in Fig. 2c,d. For nonlinear networks (high κ), we find a monotonic increase in non-affine fluctuations as the network is diluted down to p_b, where Γ exhibits a peak; this may suggest a divergence of Γ at the bending-rigidity threshold, consistent with the existence of a critical point. In addition, for smaller values of κ, a second peak in Γ develops at p_{CF} (Fig. 2c,d.). Importantly, the development of this peak coincides with the appearance of a crossover between the stretching and bending regimes (Fig. 2a–d).

The critical phenomena we observe in the mechanical behaviour indicate a divergence of the non-affine fluctuations at p_{CF} of the

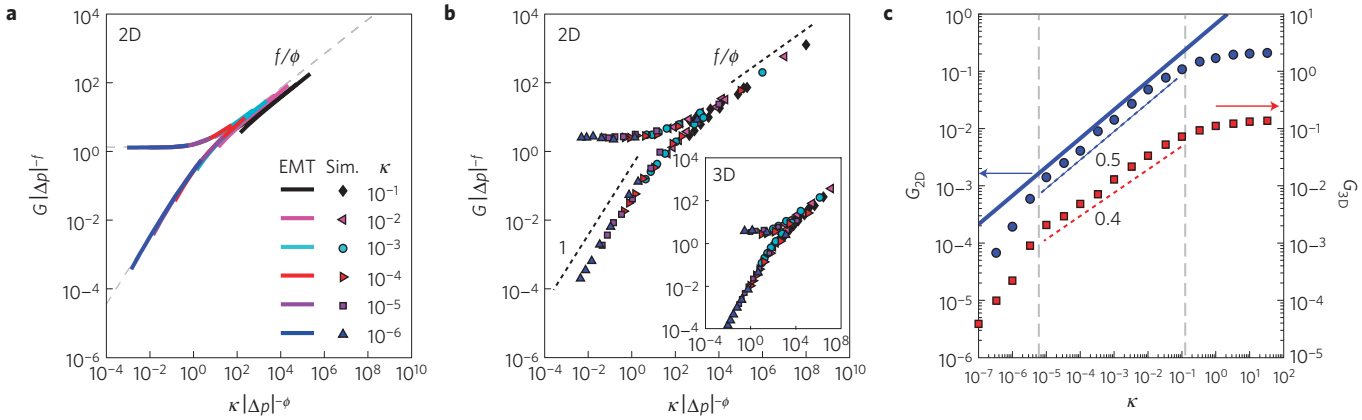

Figure 3 | Scaling analysis of the mechanics and anomalous elasticity. a,**b**, Scaling of the shear modulus, G, in the vicinity of the isostatic point with the scaling form $G|\Delta p|^{-f} = \mathcal{G}_{\pm}(\kappa|\Delta p|^{-\phi})$, with G in units of μ/ℓ_0^{d-1} and the bending rigidity, κ, in units of $\mu\ell_0^2$, for a diluted triangular lattice over a broad range of filament bending rigidities (κ in units of $\mu\ell_0^2$: 10^{-1} black, 10^{-2} magenta, 10^{-3} cyan, 10^{-4} red, 10^{-5} purple and 10^{-6} blue) for the EMT calculations (**a**) and the simulations (**b**). The asymptotic form of the scaling function for low κ is shown as a dashed grey line in **a**. The scaling for the numerical data on a three-dimensional fcc lattice is shown as an inset in **b**. The EMT exponents are $f_{CF} = 1$, $\phi = 2$. In contrast, numerically we obtain $f_{CF} = 1.4 \pm 0.1$, $\phi = 3.0 \pm 0.2$ (2D) and $f_{CF} = 1.6 \pm 0.2$ $\phi = 3.6 \pm 0.3$ (3D). The scaling for the numerical data is carried out with respect to the isostatic point of the finite system $p_{CF}(W) = 0.651$ (2D, $W = 200$) and $p_{CF}(W) = 0.473$ (3D, $W = 30$). **c**, The shear modulus as a function of κ close to the isostatic point for a triangular lattice ($p = 0.643$, blue circles) and an fcc lattice ($p = 0.47$, red squares). At low κ there is a bending-dominated regime $G_{bend} \sim \kappa$; at intermediate κ there is a regime in which stretching and bending modes couple strongly with $G \sim \mu^{1-x}\kappa^x$, where $x = 0.50 \pm 0.01$ (2D) and $x \approx 0.40 \pm 0.01$ (3D). The EMT calculation for $\kappa/\mu \gg |\Delta p|^{\phi}$ is shown as a solid blue line.

form $\Gamma = \Gamma_{\pm}|\Delta p|^{-\lambda_{CF}}$, similar to that of spring networks in a jammed configuration[12]. To investigate the nature of the cusp in Γ at p_{CF} we exploit the finite size of the fibre network, W, in our simulations[48]. In particular, we anticipate an emergent correlation length $\xi = \xi_{\pm}|\Delta p|^{-\nu_{CF}}$—diverging at p_{CF} for vanishing κ—which is associated with the divergent strain fluctuations. However, this divergence of ξ is limited by the system size, thereby suppressing the divergence of Γ. More specifically, the suppression of the divergent correlation length ξ is predicted to result in a system-size-dependent shift of Δp by an amount Δp^*, which is determined by $W \simeq \xi_{max} = \xi_{\pm}|\Delta p^*|^{-\nu_{CF}}$. Indeed, we find that the location of the peak in Γ shifts towards higher p with increasing W according to $p_{CF}(W) = p_{CF} + bW^{-1/\nu_{CF}}$, with $p_{CF} = 0.659 \pm 0.002$, $b = -0.3 \pm 0.1$ and $\nu_{CF} = 1.4 \pm 0.2$ (Supplementary Information); these values for ν_{CF} and p_{CF} are consistent with previous results on pure CF networks where $\kappa = 0$ (refs 35,49). In addition, the amplitude of the maximum in Γ increases with system size (Fig. 4a), in quantitative accord with the expected finite-size scaling $\Gamma_{max} \sim |\Delta p^*|^{-\lambda_{CF}} \sim W^{-\lambda_{CF}/\nu_{CF}}$. Moreover, we find a good collapse of the simulation data with $\Gamma = W^{\lambda_{CF}/\nu_{CF}}\mathcal{F}_{\Gamma,\pm}(|\Delta p|W^{1/\nu_{CF}})$ over a range of system sizes, with $\lambda_{CF}/\nu_{CF} = 1.6 \pm 0.2$ and $\nu_{CF} = 1.4 \pm 0.2$, as shown in Fig. 4b.

The shear modulus also exhibits such finite-size scaling (Supplementary Information) according to $G = W^{-f_{CF}/\nu_{CF}}\mathcal{F}_{G,\pm}(|\Delta p|W^{1/\nu_{CF}})$, consistent with the presence of a diverging correlation length ξ, as shown in Fig. 4c. We obtain a good collapse of the elasticity data using $f_{CF}/\nu_{CF} = 0.9 \pm 0.1$, along with ν_{CF} determined from the finite-size scaling of Γ (Fig. 4b and Supplementary Information); these findings are consistent with the value of f_{CF} obtained from the scaling in Fig. 3. This finite-size scaling analysis for both the strain fluctuations and the shear modulus at p_{CF} provides evidence for the existence of a diverging correlation length.

We find analogous finite-size scaling behaviour in the vicinity of the fibre-bending threshold p_b. In particular, the non-affinity parameter Γ diverges at the bending threshold p_b when $\kappa > 0$, and both Γ and G exhibit finite-size scaling at p_b, enabling us to extract a correlation length. The associated critical exponents we calculate are $\lambda_b = 1.8 \pm 0.3$, $\nu_b = \pm 0.2$ and $f_b = 3.2 \pm 0.4$ ($f_b = 1$ in our EMT) for small κ. This places our fibre model, along with the two-dimensional model ($f_b \simeq 3$; refs 17,18) in a different universality class from bond-bending models, for which $f_b = 3.97$ (ref. 34). In summary, at both the CF stretching and bending thresholds, we find critical behaviour that is accompanied by divergent non-affine fluctuations and a scale-dependent shear modulus, implying a breakdown of continuum elasticity below the divergent length scale ξ.

Table 1 | Critical exponents.

Exponent	2D sim.	2D EMT	3D sim.
f_{CF}	1.4 ± 0.1	1	1.6 ± 0.2
ϕ	3.0 ± 0.2	2	3.6 ± 0.3
ν_{CF}	1.4 ± 0.2		
λ_{CF}	2.2 ± 0.4		
f_b	3.2 ± 0.4	1	2.3 ± 0.2
ν_b	1.3 ± 0.2		
λ_b	1.8 ± 0.3		

The undiluted triangular and fcc lattices we study have a coordination number greater than $2d$, the Maxwell CF isostatic threshold. These networks consist of infinitely long straight filaments. Cutting bonds as we do introduces both finite-length polymers, and lower connectivity, down to the CF threshold and below. As a result, our model exhibits two thresholds at p_{CF} and p_b (Fig. 5), in contrast to previous Mikado models in 2D (refs 17,18,20) and network glass models[27], which only exhibit the bending-rigidity threshold. Cytoskeletal and extracellular networks can have z as low as 3 (for example, in branched networks) and as high as 6 (in the case of actin–spectrin networks), although they typically have a local connectivity near $z = 4$, where two filaments are connected by a crosslink, well below the naive CF threshold. However, in such networks there can be rigid crosslinks that fix a preferred angle[5,7,16] or significant internal stresses, originating from the network gelation process[14], both of which can shift the bending-rigidity threshold to lower connectivity values[22]. Moreover, for networks with straight fibres such as those considered here but with $z \leq 4$, internal stresses generated by molecular motors can induce a transition from a bending- to a stretching-dominated

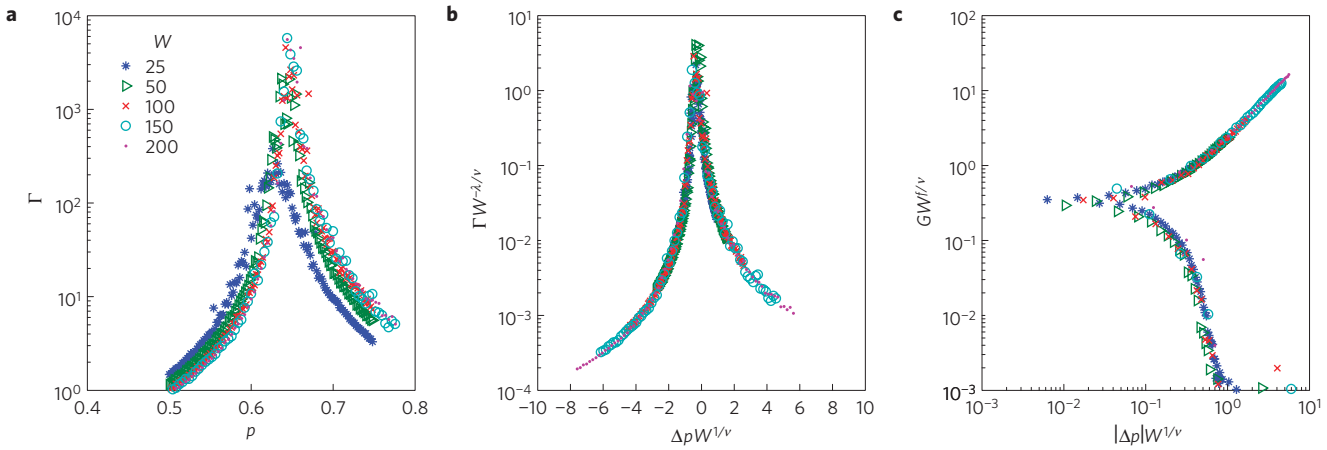

Figure 4 | Finite-size scaling. a, The non-affinity measure, Γ, for a two-dimensional triangular lattice at $\kappa = 0$ for various system sizes, W. **b**,**c**, Finite-size scaling of Γ according to the scaling form $\Gamma = W^{\lambda_{CF}/\nu_{CF}} \mathcal{F}_{\Gamma,\pm}(\Delta p W^{1/\nu_{CF}})$ (**b**) and of the shear modulus with the scaling form $G = W^{-f/\nu_{CF}} \mathcal{F}_{G,\pm}(|\Delta p| W^{1/\nu_{CF}})$ (**c**). Here $\Delta p = p - p_{CF}$, where $p_{CF} = 0.659 \pm 0.002$ in the limit $W \to \infty$. The exponents we obtain are $\lambda_{CF}/\nu_{CF} = 1.6 \pm 0.2$, $\nu_{CF} = 1.4 \pm 0.2$ and $f_{CF}/\nu_{CF} = 0.9 \pm 0.1$.

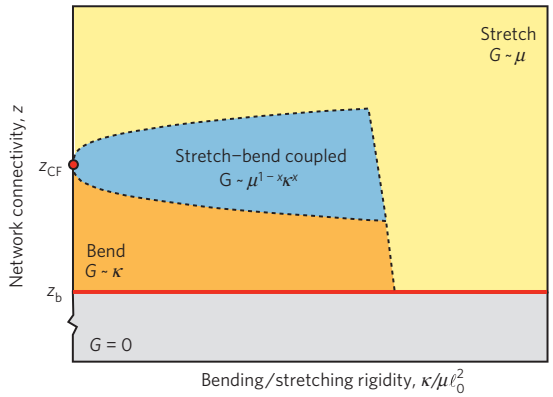

Figure 5 | Phase diagram. The phase diagram for diluted fibre networks with connectivities that cover both the CF and bending thresholds. Above the bending-rigidity percolation point, z_b, there are three distinct mechanical regimes: a stretching-dominated regime, with $G \sim \mu$, a bending-dominated regime, with $G \sim \kappa$, and a regime in which bend and stretch modes couple, with $G \sim \mu^{1-x}\kappa^x$. Here x is related to the critical exponents, $x = f/\phi$. We find here that $x = 0.50 \pm 0.01$ (two-dimensional triangular lattice) and $x = 0.40 \pm 0.01$ (three-dimensional fcc). The mechanical regimes are controlled by the CF isostatic point, z_{CF}, which acts as a zero-temperature critical point.

network elasticity[33]. We conjecture that such systems may exhibit a stress-reduced CF threshold and a concomitant stretch–bend crossover behaviour analogous to what we observe here, including anomalous scaling for the network elasticity (Fig. 5). In addition, we expect that our results for the crossover behaviour will apply to bond-bending models on similar lattices to ours for rigidity percolation[10,27,31,32] and network glasses that include bending forces between bond pairs at each network node.

Finally, from the perspective of critical phenomena more generally, the kind of crossover behaviour we find here is in contrast to most thermal systems, where a field or coupling constant leads to a crossover from one critical system to another, such as from the Heisenberg model to the Ising model[48]. In such systems, there is a continuous evolution of the critical point that is governed by the crossover exponent ϕ. Interestingly, we find no such continuous evolution with varying bending rigidity, but rather a discontinuous jump in the critical point p_c as soon as κ becomes non-zero, consistent with observations in bond-bending[25] and Born models[24].

Methods

Simulations. The mechanical response of the network is determined in our simulations by applying a shear deformation with a strain γ. This is realized by translating the horizontal boundaries to which the filaments are attached, after which the internal degrees of freedom are relaxed by minimizing the energy using a conjugate-gradient algorithm. To reduce edge effects in our simulation, periodic boundary conditions are employed at all boundaries. The shear modulus of the network is related to the elastic energy through $G = (2/V)(E/\gamma^2)$ for a small strain γ, where V is the area/volume of the system. In these simulations we have used system sizes of $W^2 \approx 40{,}000$ (2D) and $W^3 \approx 30{,}000$ (3D) unless stated otherwise, and we use strains no larger than $\gamma = 0.05$.

EMT. The EMT maps the diluted random network to an undiluted uniform effective medium (EM) in which all the fibres have a stretching modulus μ_m and a bending rigidity κ_m, which are determined self-consistently as outlined below. In our theory, κ is a property of the filament connecting neighbouring sites rather than a site-associated rigidity that connects next-nearest-neighbour sites. Following standard EM procedures[11,41], an arbitrary bond is either replaced with probability p by a bond of stretching modulus μ and bending rigidity κ or removed with probability $1-p$. The phonon Green function $\mathbf{G}^V$ after this replacement is calculated perturbatively from the uniform EM Green function $\mathbf{G}$, treating the replaced bond as a scattering potential V on the EM Hamiltonian,

$$\mathbf{G}^V = \mathbf{G} + \mathbf{GTG}$$

where the $\mathbf{T}$ matrix represents all multiple-scattering contributions from the chosen bond[39]. The EMT self-consistency condition requires that the disorder-averaged Green function is equal to that of the unperturbed EM, implying

$$p\mathbf{T}(\mu,\kappa) + (1-p)\mathbf{T}(0,0) = 0 \qquad (2)$$

which provides us with a set of equations from which μ_m and κ_m can be determined for given p.

In the EMT scattering potential V, the stretching term is simply proportional to $\mu - \mu_m$ if the bond is occupied and $-\mu_m$ if it is removed. The bending terms, however, must be treated differently because replacing a single bond generates two bending terms, both of which involve second-neighbour interactions. This can be understood by considering four sites $ijkl$ along a filament. If we replace bond jk, two bending terms involving second neighbours ijk and jkl are generated in V. The coefficients of these two bending terms can be found by considering a composite filament connecting $ijkl$ that is composed of rods with bending rigidity κ_s between sites jk and κ_m between sites ij and kl, respectively, where $\kappa_s = \kappa$ if the bond is occupied and $\kappa_s = 0$ if it is removed. A direct calculation of the minimum bending energy yields the effective bending rigidity

$$\kappa_c = 2\left(\frac{1}{\kappa_s} + \frac{1}{\kappa_m}\right)^{-1} \qquad (3)$$

and thus the coefficient of the two bending terms in the scattering potential V, involving ijk and jkl, is given by $\kappa_c - \kappa_m$.

To close the EMT self-consistency equation (2), a third-neighbour coupling λ_m

$$\frac{1}{2}\lambda_m \sum_{\langle ijkl \rangle} \left[(\mathbf{u}_{jk} - \mathbf{u}_{ij}) \times \hat{\mathbf{r}}_{ij} \right] \cdot \left[(\mathbf{u}_{kl} - \mathbf{u}_{jk}) \times \hat{\mathbf{r}}_{kl} \right]$$

must be introduced to the EM and to V accordingly. Thus the EM is characterized by three parameters $(\mu_m, \kappa_m, \lambda_m)$, determined by the self-consistency equation (2). We obtained asymptotic solutions to this equation for small κ in the vicinity of the CF isostatic point, in which the EM shear modulus $G = \sqrt{3}\mu_m/4$ can be written as a scaling function of the form of equation (1) with

$$\mathcal{G}_{\pm}(y) \simeq \frac{3}{2}\left(\pm 1 + \sqrt{1 + 4\mathcal{A}y/9} \right)$$

where $\mathcal{A} \simeq 2.413$.

For $\kappa/\mu\ell_0^2 \ll |\Delta p|^{\phi}$, to leading order, the value for μ_m reduces to $3\mu|\Delta p|$ for $\Delta p > 0$, and $(\mathcal{A}/3\ell_0^2)\kappa|\Delta p|^{-1}$ for $\Delta p < 0$. For $\kappa/\mu\ell_0 \gg |\Delta p|^{\phi}$ we find $\mu_m \simeq \sqrt{\mathcal{A}}\ell_0^{-1}\mu^{1/2}\kappa^{1/2}$. These three scaling regimes correspond to three different slopes $0, 1, 1/2$ in the $G|\Delta p|^{-f}$ versus $\kappa|\Delta p|^{-\phi}$ plot, as shown in Fig. 3a.

EMTs for bond-diluted lattices with CF springs are straightforward because the springs reside on an individual bond. In contrast, EMTs for lattices with bending forces are less so because bending forces reside on two bonds whereas the dilution procedure removes individual bonds one at a time. Our solution is to treat a given bond as a filament segment with bending modulus κ_s. The effective lattice bending modulus for neighbouring bonds with respective bending moduli κ_b and κ_m is given by equation (3). This treatment enables us to unambiguously remove one bond at a time. The resultant effective theory necessarily includes third-neighbour coupling, in contrast to a previous EMT (ref. 36), which treated the bending problem by removing two bonds at a time.

Received 1 December 2010; accepted 22 September 2011; published online 30 October 2011

References

1. Chawla, K. K. *Fibrous Materials* (Cambridge Univ. Press, 1998).
2. Kabla, A. & Mahadevan, L. Nonlinear mechanics of soft fibrous networks. *J. R. Soc. Interface* **4,** 99–106 (2007).
3. Hough, L. A., Islam, M. F., Janmey, P. A. & Yodh, A. G. Viscoelasticity of single wall carbon nanotube suspensions. *Phys. Rev. Lett.* **93,** 168102 (2004).
4. Hall, L. J. *et al.* Sign change of Poisson's ratio for carbon nanotube sheets. *Science* **320,** 504–507 (2008).
5. Bausch, A. R. & Kroy, K. A bottom-up approach to cell mechanics. *Nature Phys.* **2,** 231–238 (2006).
6. Fletcher, D. A. & Mullins, R. D. Cell mechanics and the cytoskeleton. *Nature* **463,** 485–492 (2010).
7. Kasza, K. E. *et al.* The cell as a material. *Curr. Opin. Cell Biol.* **19,** 101–107 (2007).
8. Pedersen, J. A. & Swartz, M. A. Mechanobiology in the third dimension. *Ann. Biomed. Eng.* **33,** 1469–1490 (2005).
9. Maxwell, J. C. On the calculation of the equilibrium and stiffness of frames. *Phil. Mag.* **27,** 294–299 (1864).
10. Thorpe, M. F. Continuous deformations in random networks. *J. Non-Cryst. Solids* **57,** 355–370 (1983).
11. Garboczi, E. J. & Thorpe, M. F. Effective-medium theory of percolation on central-force elastic networks. III. The superelastic problem. *Phys. Rev. B* **33,** 3289–3294 (1986).
12. Wyart, M., Liang, H., Kabla, A. & Mahadevan, L. Elasticity of floppy and stiff random networks. *Phys. Rev. Lett.* **101,** 215501 (2008).
13. Gardel, M. L. *et al.* Elastic behavior of cross-linked and bundled actin networks. *Science* **304,** 1301–1305 (2004).
14. Storm, C., Pastore, J. J., MacKintosh, F. C., Lubensky, T. C. & Janmey, P. A. Nonlinear elasticity in biological gels. *Nature* **435,** 191–194 (2005).
15. Chaudhuri, O., Parekh, S. H. & Fletcher, D. A. Reversible stress softening of actin networks. *Nature* **445,** 295–298 (2007).
16. Lieleg, O., Claessens, M. M. A. E., Heussinger, C., Frey, E. & Bausch, A. R. Mechanics of bundled semiflexible polymer networks. *Phys. Rev. Lett.* **99,** 088102 (2007).
17. Head, D. A., Levine, A. J. & MacKintosh, F. C. Deformation of cross-linked semiflexible polymer networks. *Phys. Rev. Lett.* **91,** 108102 (2003).
18. Wilhelm, J. & Frey, E. Elasticity of stiff polymer networks. *Phys. Rev. Lett.* **91,** 108103 (2003).
19. Onck, P. R., Koeman, T., van Dillen, T. & van der Giessen, E. Alternative explanation of stiffening in cross-linked semiflexible networks. *Phys. Rev. Lett.* **95,** 178102 (2005).
20. Heussinger, C. & Frey, E. Floppy modes and nonaffine deformations in random fiber networks. *Phys. Rev. Lett.* **97,** 105501 (2006).
21. Buxton, G. A. & Clarke, N. Bending to stretching transition in disordered networks. *Phys. Rev. Lett.* **98,** 238103 (2007).
22. Huisman, E. M. & Lubensky, T. C. Internal stresses, normal modes, and nonaffinity in three-dimensional biopolymer networks. *Phys. Rev. Lett.* **106,** 088301 (2011).
23. Jacobs, D. J. & Thorpe, M. F. Generic rigidity percolation in two dimensions. *Phys. Rev. E* **53,** 3682–3693 (1996).
24. Feng, S. & Sen, P. N. Percolation on elastic networks: New exponent and threshold. *Phys. Rev. Lett.* **52,** 216–219 (1984).
25. Feng, S., Sen, P. N., Halperin, B. I. & Lobb, C. J. Percolation on two-dimensional elastic networks with rotationally invariant bond-bending forces. *Phys. Rev. B* **30,** 5386–5389 (1984).
26. Phillips, J. C. Topology of covalent non-crystalline solids II: Medium-range order in chalcogenide alloys and A–Si(Ge). *J. Non-Cryst. Solids* **43,** 37–77 (1981).
27. He, H. & Thorpe, M. F. Elastic properties of glasses. *Phys. Rev. Lett.* **54,** 2107–2110 (1985).
28. Liu, A. J. & Nagel, S. R. Nonlinear dynamics: Jamming is not just cool any more. *Nature* **396,** 21–22 (1998).
29. O'Hern, C. S., Silbert, L. E., Liu, A. J. & Nagel, S. R. Jamming at zero temperature and zero applied stress: The epitome of disorder. *Phys. Rev. E* **68,** 011306 (2003).
30. Liu, A. J., Nagel, S. R., van Saarloos, W. & Wyart, M. in *Dynamical Heterogeneities in Glasses, Colloids, and Granular Media* (eds Berthier, L., Biroli, G., Bouchaud, J-P., Cipeletti, L. & van Saarloos, W.) (Oxford Univ. Press, 2010).
31. Schwartz, L. M., Feng, S., Thorpe, M. F. & Sen, P. N. Behavior of depleted elastic networks: Comparison of effective-medium and numerical calculations. *Phys. Rev. B* **32,** 4607–4617 (1985).
32. Sahimi, M. & Arbabi, S. Mechanics of disordered solids. II. Percolation on elastic networks with bond-bending forces. *Phys. Rev. B* **47,** 703–712 (1993).
33. Broedersz, C. P. & MacKintosh, F. C. Molecular motors stiffen non-affine semiflexible polymer networks. *Soft Matter* **7,** 3186–3191 (2011).
34. Zabolitzky, J. G., Bergman, D. J. & Stauffer, D. Precision calculation of elasticity for percolation. *J. Stat. Phys.* **44,** 211–223 (1986).
35. Arbabi, S. & Sahimi, M. Mechanics of disordered solids. I. Percolation on elastic networks with central forces. *Phys. Rev. B* **47,** 695–702 (1993).
36. Das, M., MacKintosh, F. C. & Levine, A. J. Effective medium theory of semiflexible filamentous networks. *Phys. Rev. Lett.* **99,** 038101 (2007).
37. Lax, M. Multiple scattering of waves. *Rev. Mod. Phys.* **23,** 287–310 (1951).
38. Elliott, R. J., Krumhansl, J. A. & Leath, P. L. The theory and properties of randomly disordered crystals and related physical systems. *Rev. Mod. Phys.* **46,** 465–543 (1974).
39. Soven, P. Contribution to the theory of disordered alloys. *Phys. Rev.* **178,** 1136–1144 (1969).
40. Mao, X., Xu, N. & Lubensky, T. C. Soft modes and elasticity of nearly isostatic lattices: Randomness and dissipation. *Phys. Rev. Lett.* **104,** 085504 (2010).
41. Feng, S., Thorpe, M. F. & Garboczi, E. Effective-medium theory of percolation on central-force elastic networks. *Phys. Rev. B* **31,** 276–280 (1985).
42. Straley, J. Critical phenomena in resistor networks. *J. Phys. C* **9,** 783–795 (1976).
43. Dykhne, A. M. Conductivity of a two-dimensional two-phase system. *JETP* **32,** 63–65 (1971).
44. Efros, A. L. & Shklovskii, B. I. Critical behaviour of conductivity and dielectric constant near the metal–non-metal transition threshold. *Phys. Status Solidi B* **76,** 475–485 (1976).
45. Heussinger, C. & Frey, E. Stiff polymers, foams, and fiber networks. *Phys. Rev. Lett.* **96,** 017802 (2006).
46. DiDonna, B. A. & Lubensky, T. C. Nonaffine correlations in random elastic media. *Phys. Rev. E* **72,** 066619 (2005).
47. Liu, J., Koenderink, G. H., Kasza, K. E., MacKintosh, F. C. & Weitz, D. A. Visualizing the strain field in semiflexible polymer networks: Strain fluctuations and nonlinear rheology of *f*-actin gels. *Phys. Rev. Lett.* **98,** 198304 (2007).
48. Fisher, M. E. in *Proc. School on Critical Phenomena, Stellenbosch, South Africa, 1982* Vol. 186 (ed. Hahne, F. J. W.) (Springer, 1983).
49. Chubynsky, M. V. & Thorpe, M. F. Algorithms for three-dimensional rigidity analysis and a first-order percolation transition. *Phys. Rev. E* **76,** 041135 (2007).

Acknowledgements

This work was supported in part by NSF-DMR-0804900 (T.C.L. and X.M.) and in part by FOM/NWO (C.P.B. and F.C.M.). The authors thank M. Wyart, M. Das and L. Jawerth for useful discussions.

Author contributions

C.P.B. and F.C.M. designed the simulation model, which was developed and executed by C.P.B.; X.M. and T.C.L. developed and executed the EMT. All authors contributed to the writing of the paper.

Additional information

The authors declare no competing financial interests. Supplementary information accompanies this paper on www.nature.com/naturephysics. Reprints and permissions information is available online at http://www.nature.com/reprints. Correspondence and requests for materials should be addressed to T.C.L. or F.C.M.